Non-Data-Aided Symbol Rate Estimation for a Low Roll-Off Factor Nyquist WDM Signal

Fangqi Shen , Zhiping Huang, and Junhao Ba

Abstract—Nyquist signals with low roll-off factors pose a challenge for non-data-aided blind symbol rate estimation problems in long-haul applications. We adopted the nonlinear least squares (NLS) approach to estimate the symbol rate of low roll-off factor signals. This method tolerates chromatic dispersion and additive Gaussian noise. In addition, this method can operate below two samples per symbol, thus enabling low-power-consumption receivers. Simulation and experimental results show that the mean squared error is below 10^{-4} with only 3000 samples needed for polarization-division-multiplexed (PDM) quadrature phase-shift keying (QPSK) or quadrature amplitude modulation (QAM) systems with a roll-off factor below 0.1 for an optical signal-to-noise ratio greater than 12 dB. Compared with the maximum likelihood estimation (MLE) method, our proposed method has a more robust performance under low roll-off factor signals and in low-sampling-rate scenarios. The mean squared error remains the same for a nominal symbol rate (i.e., the ratio of the symbol rate to the sampling rate, also widely known as oversampling rate) ranging from 0.1 to 0.9.

Index Terms—Frequency estimation, nonlinear least squares estimation, non-data-aided.

I. INTRODUCTION

THE emergence of coherent receivers has significantly extended the flexibility and capacity of optical communication by introducing digital signal processing (DSP). With the support of DSP, the elastic optical network has quickly gained attention as it pushes spectral efficiency to new limits [1]. Meanwhile, transmission parameters like symbol rate, modulation format etc. in EON are adjusted dynamically under varying channel condition and traffic demands for the sake of maximum spectral and energy efficiency [2]. The nodes in the elastic optical network must be obtained to determine the symbol rate, modulation format, and central frequency on demand [3]. As shown in Fig. 1, symbol rate estimation is the first and foremost problem for a blind signal processing procedure because the following algorithms operate at symbol intervals.

Cyclostationary methods are well known for their communication signal timing recovery algorithms [4]. These methods utilize the cyclostationary property to detect the symbol rate.
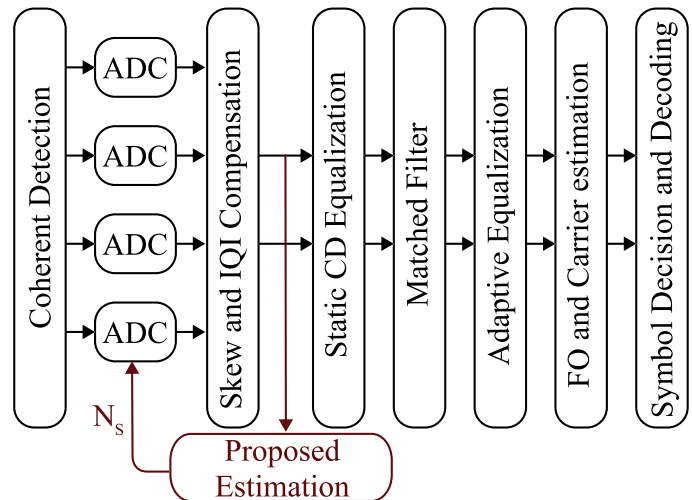
Fig. 1. Structure of the signal processing chain in a symbol rate variable receiver. Four ADCs sample the signal after coherent detection. Then, timing skew mismatch and IQ imbalance (IQI) are compensated for after the data acquisition. The proposed technique estimates N_s and uses the information to change the sampling rate of the ADC.

However, the main problem in adapting these methods to fiber communication is the fact that fiber impairments, including chromatic dispersion (CD) and polarization mode dispersion (PMD), obscure this feature [5]. Moreover, recent studies [6] show that pulse shaping with a low roll-off factor is feasible for the dense wavelength-division multiplexed (WDM) system, which is also known as the Nyquist WDM system. For a roll-off factor as low as 0.01, it takes 2^{20} samples for the cyclostationary-based method to achieve a robust evaluation since these signals have weak cyclostationary features even without the fiber impairments [7]. Evaluating the symbol rate for the Nyquist WDM system in a dispersion-unmanaged link is still an open topic.

Our previous work showed that the autocorrelation function tolerates the CD and that the symbol rate could be evaluated by applying a nonlinear operator to the sample autocorrelation [8]. However, this method does not work for low roll-off signals and less than twice the symbol rate sampling cases.

In this article, a symbol estimation method is proposed using nonlinear least squares (NLS) estimation. The main contribution of this work is that we analytically show that autocorrelation of sampled signal is proportional to that of the pulse shape function. The autocorrelation function tolerates the CD and is feasible for the least squares method. The key benefit of this method is its compatibility with low roll-off signals in the presence of CD.

Moreover, one can analytically show this method insensitive to amplifier noise and laser phase noise. It has been compared our method using simulation and experimental results with the maximum likelihood estimation (MLE) method [9]. The mean squared error (MSE) is below 10^{-4} for an optical signal-to-noise ratio (OSNR) greater than 12 dB for nominal symbol rate $N_s = 0.357$ and 0.526.

II. RELATED WORKS

Asynchronous sampling technique that uses low-sampling-rate devices such as eye pattern analyzer is attractive since the symbol rate of optical communication is relatively high. The asynchronous amplitude autocorrelation [10]–[12] and asynchronous two-tap plot [13]–[15] can be used for symbol rate estimation. However, these methods perform better for return-to-zero modulation formats with limited residue chromatic dispersion (up to 1600 ps/nm in [10]).

The cyclostationary-based method starts with the observation that a communication signal can generate a clock tone with nonlinear operators [16], [17]. Further performance analyses in [18]–[21] show that the optimal spectral line would be generated after quadratic time-invariance (QTI) transformation. This process is realized by a pair of in-phase and quadrature matched filters, following squarers for each and an adder summing the outputs of squarers. Statistical tests for the presence of cyclostationarity are derived in [22]. Symbol rate estimation using the cyclic correlation is given in [23]. The convergence rate of the cyclic correlation estimator is given in [24].

Another category of estimation methods is the blind matching method [25], [26]. The input signal is tentatively filtered with a matched filter with different parameters. The symbol rate is estimated by filter with the largest output power. These methods suit a low SNR scenario, such as that of satellite video broadcasting. However, if the roll-off factor is unknown, the error could lead to inaccurate estimations.

Owing to statistically optimal property, the MLE method becomes appealing. The main obstacle is the unknown parameter in the model, as mentioned in [24]. If the transmitted symbol is known at the receiver side, the expectation-maximization method can estimate the symbol rate in the low SNR case [27]. To simplify the model, the Gaussian MLE method treats unknown parameters as Gaussian random variables while the maximum likelihood function can be derived using the conditional expectation. Interestingly, the MLE in the Gaussian sense [9] contains both cyclic correlation and match filtering terms and gives a better result than can be achieved by the original methods.

III. PROBLEM STATEMENT

LIST OF NOTIONS

$x(t)$	Input signal
s_n	Information symbol bits
$g(t)$	Pulse shape function
β	Roll-off factor
T	Symbol duration
T_s	Sample interval
ϵ	Timing offset
ϕ	Carrier frequency offset
$n(t)$	Gaussian noise
$\delta(t)$	Dirac delta function
N_s	Nominal symbol rate
$r_{xx}(k)$	Autocorrelation function of $x(t)$
$D(\omega)$	Transfer function of chromatic dispersion
β_2	Dispersion parameter
z	Transmission distance

For a polarization-division multiplexed (PDM) system, the baseband signal for each polarization can be described as:

$$x(k) = \sum_{n=-\infty}^{\infty} s_n g(kT_s - nT + \epsilon)e^{j\phi k} + n(k). \quad (1)$$

where $\{s_n\}$ is the sequence of information symbols, $g(\cdot)$ is the pulse shape function, T is the symbol duration, T_s is the sample interval, and $n(\cdot)$ is the noise. ϵ and ϕ are the timing offset and carrier frequency offset, respectively.

The following assumptions are made in this paper:
1) The nominal symbol rate $N_s \doteq T_s/T$ is assumed to be unknown, and we can find a sufficiently accurate rational approximation $N_s \approx p/q$ referring to Diophantine approximation, where p and q are integers. In addition, we assume that $0 < N_s < 1$.
2) $g(\cdot)$ is a square-root-raised-cosine pulse with a roll-off factor β ($0 \leq \beta \leq 1$) and a symbol rate $1/T$, which is the same as in [28].
3) s_n is the zero mean, and $\mathbf{E}(s_k s_l^*) = \delta(k - l)$, where $\delta(t)$ is the Dirac delta function.
4) $n(\cdot)$ is the zero mean, white, and uncorrelated with $\{s_n\}$ and follows $\mathcal{N}(0, \sigma_w^2)$.

Our focus is on the general non-data-aided case: estimating N_s when all other parameters $\{s_n, \beta, \epsilon, \phi\}$ are unknown at the receiver.

IV. METHOD

A. Sample Autocorrelation of the Linear Modulated Signal

For N input samples $\{x(k), k = 0, 1, \ldots, N - 1\}$, the sample autocorrelation $r_{xx}(k)$ is given by:

$$r_{xx}(k) = \begin{cases} \frac{1}{N} \sum_{i=0}^{N-1-|k|} x(i)x^*(i + k) & , |k| \leq N - 1 \\ 0 & , |k| \geq N \end{cases}. \quad (2)$$

The symbol $*$ denotes conjugation. Because $x(k)$ is a cyclostationary process with finite average power, the sample autocorrelation $\hat{r}_{xx}(k)$ converges asymptotically to $r_{xx}(k)$[29]. All four received tributaries in the coherent optical receiver can be used as the input signal due to assumption 3. For $k \neq 0$:

$$\hat{r}_{xx}(k) \doteq \lim_{N \to \infty} r_{xx}(k) \overset{m.s.s.}{=} \lim_{N \to \infty} \frac{e^{j\phi k}}{N} \sum_{i=0}^{N-1} \mathbf{E}[x(i)x^*(i + k)]$$

$$= \lim_{N \to \infty} \frac{e^{j\phi k}}{N} \sum_{i=0}^{N-1} \sum_{j=-\infty}^{\infty} g(iT_s - jT + \epsilon)g[(i + k)T_s - jT + \epsilon]$$
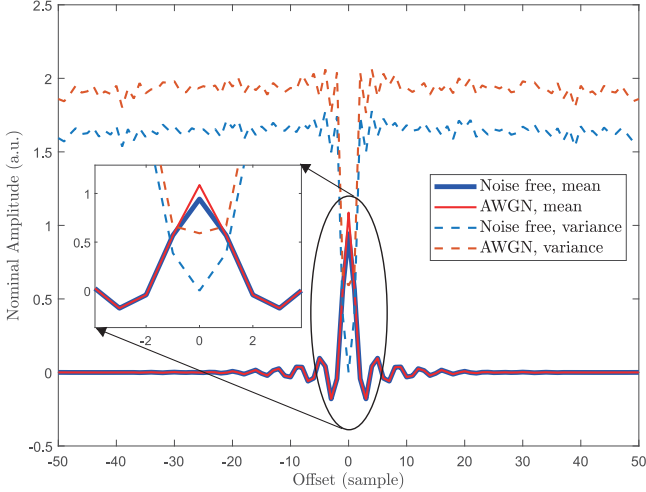
Fig. 2. Simulation results for autocorrelation of a noise-free signal and one with Gaussian noise. Nominal symbol rate $N_s = 0.53$, BPSK, and OSNR(0.5 nm) = 14 dB.

$$\approx \lim_{N \to \infty} \frac{e^{j\phi k}}{N} \sum_{i=0}^{N-1} \sum_{j=-\infty}^{\infty} g\left[\left(i - j\frac{p}{q}\right)T_s + \epsilon\right]$$

$$g\left[\left(i + k - j\frac{p}{q}\right)T_s + \epsilon\right]$$

$$\propto e^{j\phi k} \sum_{m=0}^{q-1} \sum_{n=-\infty}^{\infty} g(nT_s + mT_s/q + \epsilon)g[(n + k)T_s + mT_s/q + \epsilon]$$

$$\propto e^{j\phi k} \sum_{m=-\infty}^{\infty} g(mT_s/q + \epsilon)g(mT_s/q + kT_s + \epsilon). \quad (3)$$

where m and n are integers. The sample autocorrelation approximates the normal distribution using the *strong law of the large number* (see [29]). The green dashed line in Fig. 2 shows that the noise increases the variance; the expectation is the same for $k \neq 0$. The noise will cause a peak proportional to $n(k)$ at $r_{xx}(0)$.

Equation (3) shows that $\hat{r}_{xx}(k)$ is proportional to the sampled version of the autocorrelation function of $g(t)$ with sufficiently large N. The equivalent sampling rate is p/T_s, and the delay is kT_s.

The frequency offset term ϕk in equation (3) affects the phase of the autocorrelation estimation. A well-known treatment of the frequency offset is shown in [30], which estimates the frequency offset using the phase angle of $r_{xx}(1)$. We can simply adopt this method.

The timing offset ϵ does not affect the sample autocorrelation function. This property is desirable since we care only about the nominal symbol rate N_s. A detailed proof of this property is given in Appendix.

It can be seen from (3) that a sampling rate of less than two samples per symbol does not affect the autocorrelation function if $N_s < 1$. Thus, our proposed method can estimate the symbol rate for sampling rates less than two samples per symbol.

B. The Impact of Fiber Impairments

Fiber link impairments include the fiber loss, CD, PMD, and nonlinear impairments caused by Kerr's effect. A detailed channel model is described in [31]. The transfer function of CD is given by:

$$D(\omega) = \exp\left(-j\frac{\omega^2 \beta_2 z}{2}\right). \quad (4)$$

where β_2 is the dispersion parameter and z is the transmission distance.

The impulse response of PMD has the following form:

$$a\delta(t) + b\delta(t + \text{PMD}_{\text{coeff}}\sqrt{z}). \quad (5)$$

where $\text{PMD}_{\text{coeff}}$ is the PMD coefficient.

The CD and PMD are mainly considered for several reasons. First, the fiber loss is fully compensated for with the amplifier. Second, the polarization effect with polarization-dependent loss and additional birefringence are linear combinations between two polarizations. The autocorrelation function of each polarization is the same since the signal scheme is identical for each polarization. Finally, the nonlinear impairment for a dispersion-uncompensated link behaves as Gaussian noise [32]. As the simulation shows, the required OSNR for symbol rate estimation with our proposed method is generally lower than the OSNR for advanced modulation transmission. As a result, our proposed method has a large margin for the nonlinear interference.

The CD does not affect the autocorrelation function. As a general result of the linear time-invariant system, the impact of CD $H(\omega)H^*(\omega) = 1$ on the autocorrelation function (see equation (2.195) of [33]). As a result, the autocorrelation of the input signal and that of the output signal are the same for CD. However, the cyclostationary-based method will suffer from the fading effect when the CD is left uncompensated [5], [34].

The PMD affects the autocorrelation function since it creates a low-pass 'echo' channel. In real applications, the typical $\text{PMD}_{\text{coeff}}$ of the standard single-mode fiber is 0.04 ps/$\sqrt{\text{km}}$. The mean differential group delay is approximately 0.24 ps for a link of 3600 km. The group delay can be ignored since the symbol duration of the state-of-the-art 400 Gbps Nyquist superchannel is 35 ps. It's believed that the impact of PMD is not prominent in the newly installed fiber link and confirm this in the experimental section.

C. Least Squares Problem Formulation

For a blind symbol rate estimation, the transmitted information symbols are unknown at the receiver. Lopez-Salcedo [35] and Mosquera [9] adopt the Gaussian maximum likelihood approach to solve the symbol rate estimation problem. They assume that the symbols follow a Gaussian distribution. This assumption yields a reasonable result: the maximum likelihood estimation of the symbol rate includes a cyclic correlation term (see equation (22) of [9]). However, in the presence of large accumulated CD, these methods fail to estimate the symbol rate due to the spectral fading effect of the CD [5].

As discussed above, the idea of fitting autocorrelation into estimation becomes straightforward for low CD tolerance of MLE
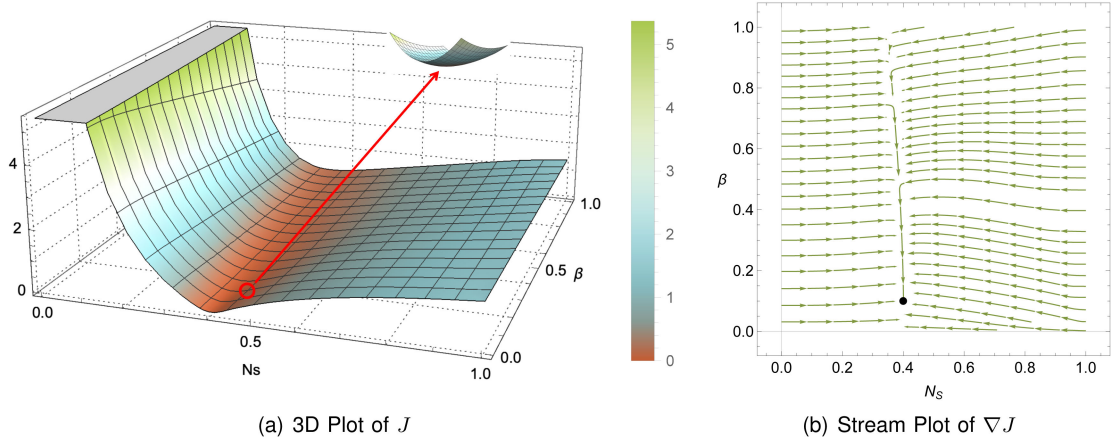
(a) 3D Plot of J

(b) Stream Plot of ∇J

Fig. 3. 3D plot (a) and stream plot of the gradient (b) of the cost function $J(\beta, N_s)$, where only parameter mismatch is the imperfection. $N_s = 0.4$, $\beta = 0.1$, and OSNR=14 dB. The details are enlarged around the true value.

method. Given low cyclostationarity the Nyquist WDM signal exhibits, NLS method is applied utilizing other characteristics to estimate symbol rate in low roll-off factor squared-root-raised-cosine (SSRC) pulse shaping scenario.

When the sampling rate T_s satisfies $T_s < T$, we can estimate N_s by solving the following least squares problem:

$$\min_{0 \leq \beta \leq 1, 0 < N_s < 1} J(\beta, N_s)$$

$$J(\beta, N_s) = \sum_{k=-L}^{L} [\hat{r}_{xx}(k) - A f(\beta, kN_s)]^2. \tag{6}$$

Under high-SNR optical communication, the scaling parameter A can be ignored as 1 by normalizing the autocorrelation with $\hat{r}_{xx}(0)$. For SRRC pulse shaping signal, one can approximate the system model $f(\beta, kN_s)$ to a raised-cosine function and express $f(\cdot)$ as:

$$f(\beta, kN_s) \approx \frac{\sin(\pi k N_s)}{\pi k N_s} \frac{\cos(\pi k \beta N_s)}{1 - (2k\beta N_s)^2}. \tag{7}$$

Fig. 3 shows an example of J in (6). Fig. 3(a) shows J when only parameter mismatches are present.

The derivative of equation (6) shows some practical properties for us to optimize J. The gradient of J is depicted (see Fig. 3(b)) and find that $\frac{\partial J}{\partial N_s} \gg \frac{\partial J}{\partial \beta}$. This property makes the optimization methods using derivative information efficient in solving this problem. We use the *trusted region reflective* method [36].

D. Parameter Initialization

Since iterative numeric optimization methods are sensitive to the initial parameters, it is desirable to carry out a fast yet less accurate evaluation. The method of moments is often used for parameter initialization [37], and we use this method as the starting point for the NLS problem.

The zeroes of the raised-cosine function (7) are independent of the scaling parameter A. It is possible to achieve a coarse estimation of N_s via the zero points. Flohberger [38] and Xu [39]
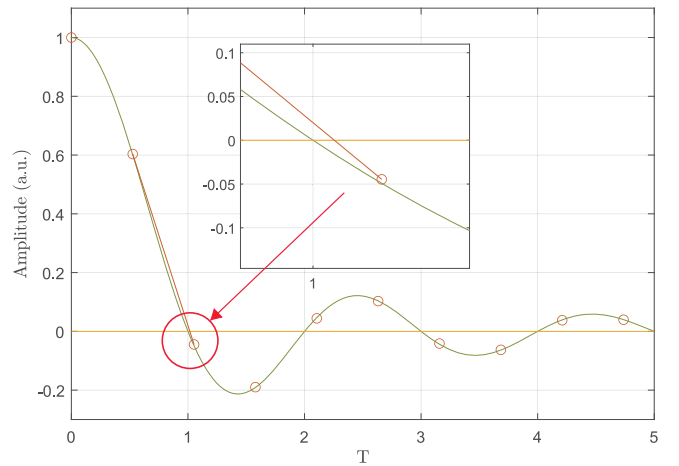

Fig. 4. An example of using linear interpolation for the zero-crossing point estimation. Nominal symbol rate $N_s = 0.53$, BPSK.

also use the Fourier interpolation technique (i.e., carrying out FFT, padding with zero, and then inverse FFT) with this property.

Because the second-order derivative is relatively small around the zero points, we may use a linear interpolation around the first zero point (see Fig. 4). We can express the initial estimation as:

$$N_{s0} = k_0 + \frac{\hat{r}_{xx}(k_0)}{\hat{r}_{xx}(k_0 + 1) - \hat{r}_{xx}(k_0)}. \tag{8}$$

where k_0 is the smallest k that satisfies the zero crossing condition, i.e., $\hat{r}_{xx}(k_0) > 0$ and $\hat{r}_{xx}(k_0 + 1) < 0$.

V. NUMERICAL AND EXPERIMENTAL RESULTS

A. Simulation Environment and Analysis Method

To study the feasibility of the proposed method, we conduct computer simulations of single-carrier PDM-QPSK signals using MATLAB. We compare our proposed method with the MLE method, which is a combination of cyclic correlation and the
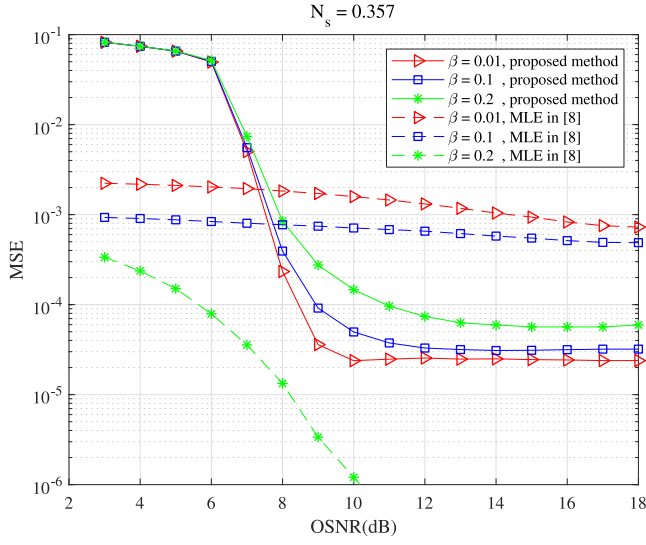
Fig. 5. Performance evaluation for the proposed NLS method and MLE in [9]. $N_s = 0.357$, and $N = 3000$. The result of our proposed method is plotted as the solid line, and the result of MLE is plotted as the dashed line.
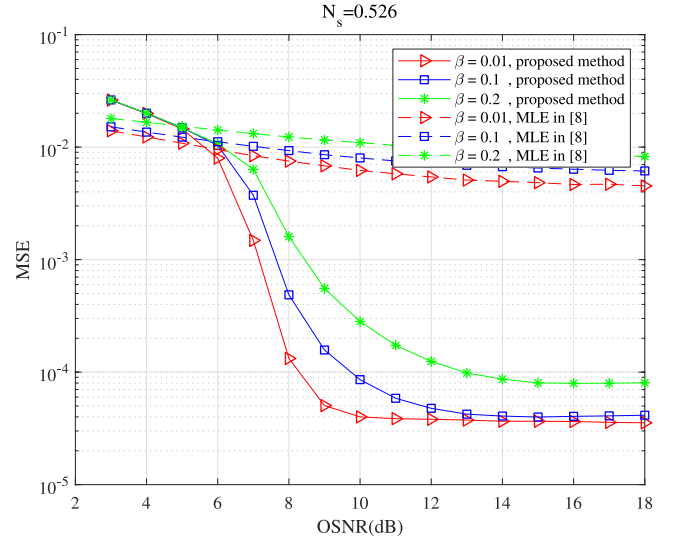

Fig. 6. Performance evaluation for the proposed NLS method and MLE in [9]. $N_s = 0.526$, and $N = 3000$. The result of our proposed method is plotted as the solid line, and the result of MLE is plotted as the dashed line.

blind matching technique. We adopt the same simulation setup as in [9].

On the signal generation side, a QPSK signal of 28 GBaud is generated using uncorrelated pseudorandom binary sequences with a length of $2^{32} - 1$. Square-root-raised-cosine pulse shaping is added using a finite impulse filter with a length of 32. To test the performance for both more than and less than two samples per symbol, we set the nominal symbol rate N_s to $\{0.357, 0.526\}$.

For each set of simulations, a total of 3×10^5 realizations are carried out to calculate the MSE performance, which is calculated as $\text{MSE} = \mathbf{E}[(N_s - \hat{N}_s)^2]$, where N_s is the exact nominal symbol rate and $\hat{N}_s$ is the estimator output. For each realization, 3000 samples are generated as the input signal.

For our proposed method, L in (6) is 50 to formulate the least squares estimation. The *fmincon* function of MATLAB is used for the least squares estimation with the default settings (the algorithm is 'trust-region reflected,' and the threshold is 1e-6).

The setting of the MLE method is the same as in [9], except for the fine search range. We expand the fine search range from $\pm 10\%$ to $\pm 50\%$ since their coarse estimation is inaccurate for N_s near 0.5.

B. MSE Performance Against the OSNR

In this set of simulations, we evaluate the performance against OSNRs ranging from 3 dB to 18 dB. The roll-off factor is set to $\{0.01, 0.1, 0.2\}$.

As shown in Fig. 5 and Fig. 6, the MSE for all cases drops below 10^{-4} as the OSNR increases to 12 dB for our proposed method. The performance when $N_s = 0.357$ is slightly better than that when $N_s = 0.526$ since the aliased out-band noise affects the performance when $N_s = 0.526$.
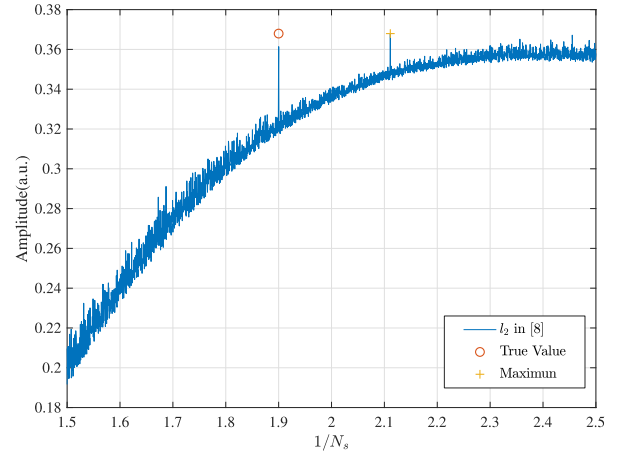

Fig. 7. Simulation results for the maximum likelihood function l_2 in [9]. The exact symbol rate N_s is $10/19$, while the aliasing effect makes $N_s = 9/19$ the largest value in the search span. The data length is 3000, and OSNR = 14 dB.

The MLE method performs better only when $N_s = 0.357$ and $\beta = 0.2$. In all other cases, our method performs better. The main reasons are as follows.

First, as the cyclic correlation decreases with the roll-off factor [7], the possibility of detection also drops. The strength of the clock tone generated by the MLE method is derived in [21], which is proportional to:

$$\int_{-\infty}^{\infty} G(f)G(f + 1/T)\mathrm{d}f. \tag{9}$$

where $G(f)$ is the Fourier transform of pulse shape function $g(t)$ and T is the symbol rate. It is straightforward to see that the clock strength depends on the interaction of the supports of $G(f)$ and $G(f + 1/T)$. In other words, the clock strength is proportional to the high frequency power (above $1/T$). When β approaches
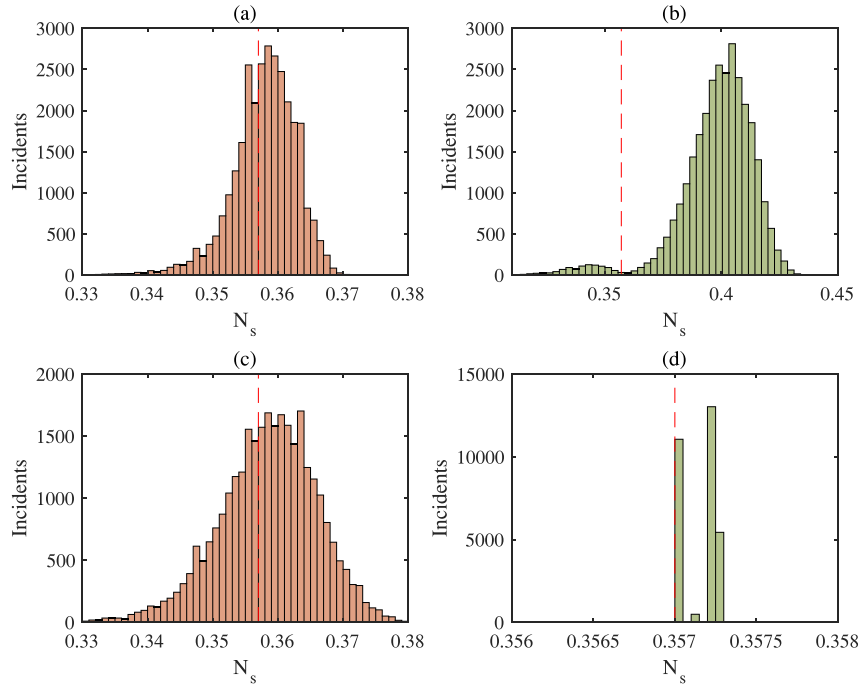
Fig. 8. Histogram of the proposed NLS method and MLE in [9]. $N_s = 0.357$, and $N = 3000$. OSNR $= 14$ dB. (a) $\beta = 0.01$ for our proposed method. (b) $\beta = 0.01$ for the MLE method. (c) $\beta = 0.2$ for our proposed method. (d) $\beta = 0.2$ for the MLE method.

Fig. 9. Histogram of the proposed NLS method and MLE in [9]. $N_s = 0.526$, and $N = 3000$. OSNR $= 14$ dB. (a) $\beta = 0.01$ for our proposed method. (b) $\beta = 0.01$ for the MLE method. (c) $\beta = 0.2$ for our proposed method. (d) $\beta = 0.2$ for the MLE method.
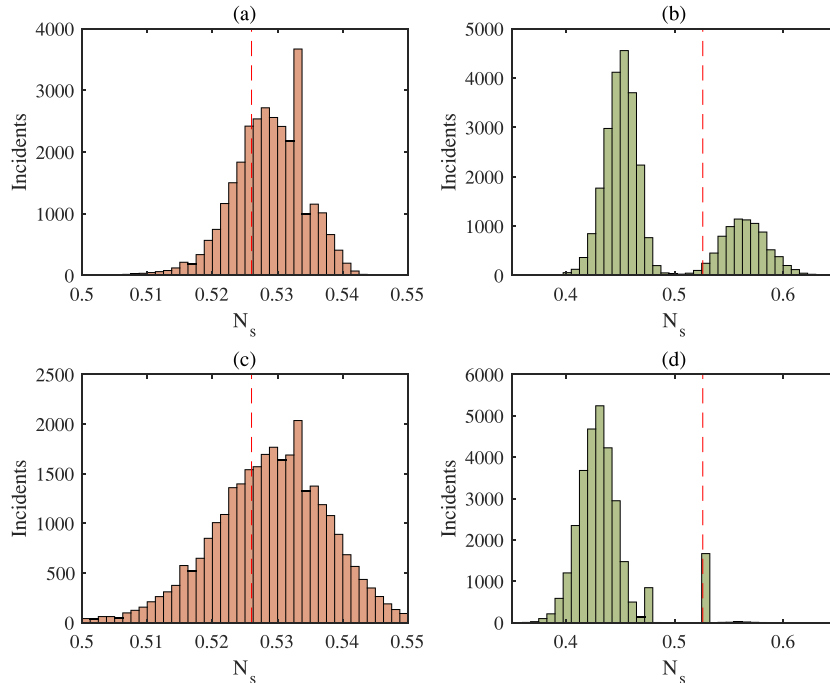
zero, the clock strength becomes zero, thus preventing the MLE method from being used.

Second, the error of the matched filter leads to inaccurate results. They adopt the impulse invariance design procedure (see [33]) for the matched filter. The aliasing effect will cause an error in the designed filter if $N_s > 1/(2 + 2\beta)$. When $N_s > 0.5$, the inevitable aliasing of the matched filter causes the error in the result. We depict the likelihood function in Fig. 7. The true N_s is $10/19$, which has an aliasing image at $9/19$. The error of the matched filter makes the baseline higher when $N_s = 9/19$.
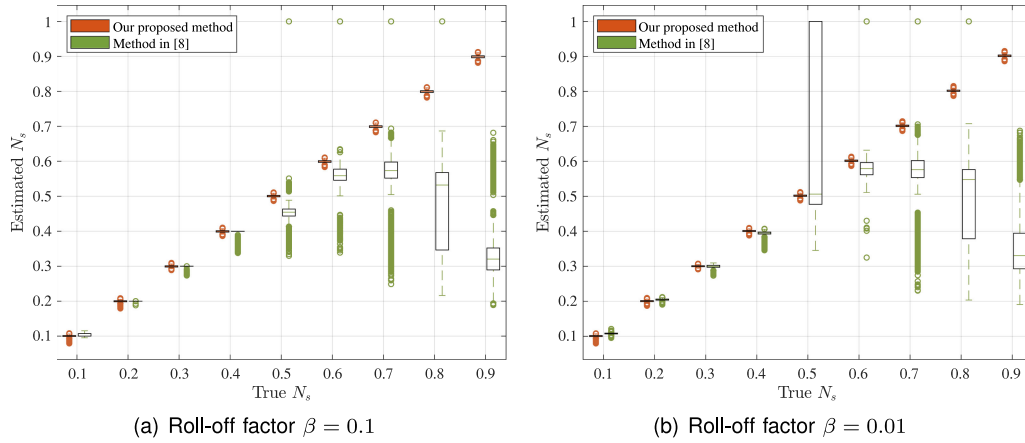
Fig. 10. Box plot for different roll-off factors $\beta = 0.1$ (a) and $\beta = 0.01$ (b). The nominal symbol rate spans from 0.1 to 0.9, and 3×10^5 realizations is simulated. OSNR = 10 dB. In each box, the central line represents the median value and the bound represents the 25th and 75th percentiles (interquartile range). The whiskers encompass 1.5 times the interquartile range.
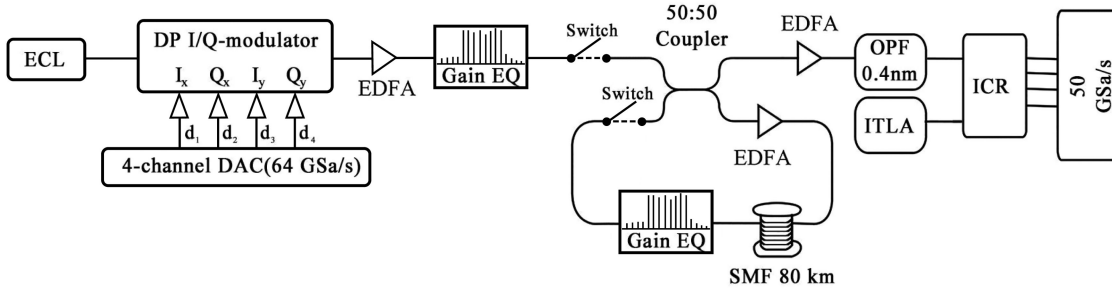

Fig. 11. Experimental evaluation setup for the symbol rate estimation on PDM-16QAM. ECL: external cavity laser. ITLA: Integrated Tunable Laser Assembly. OPF: Optical Bandpass Filter; ICR: Integrated Coherent Receiver; EDFA: Erbium-doped Fiber Amplifier.
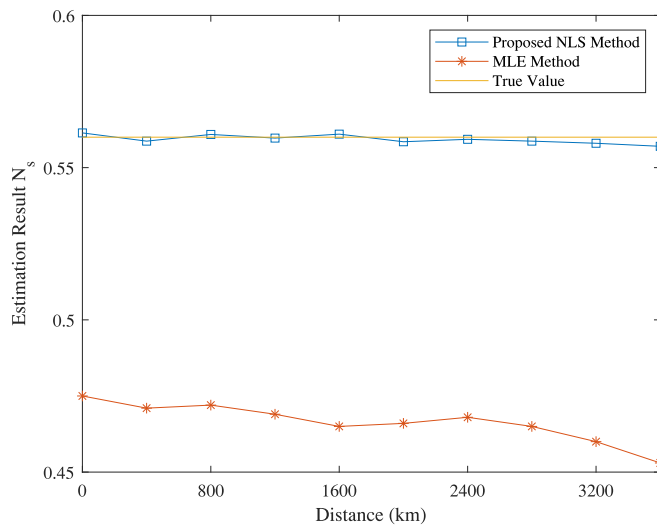

Fig. 12. Mean of the estimation results. The true value is plotted in yellow.

The histograms in Fig. 8 and Fig. 9 is depicted. Even with a large roll-off factor ($\beta = 0.2$), only ten percent of the results are correct when aliasing occurs as shown in Fig. 9(d).

Our method, by contrast, performs better when the roll-off factor is low. As β approaches zero, the accuracy increases since $g(t)$ becomes the *sinc* function, which has an infinite time support.Since the least squares estimation relies on the gradient information of the cost function J, our proposed method performs better for low roll-off factors.

The aliasing effect could also affect our proposed method. In Fig. 9(a) and (c), there is a peak around 0.536. This is referred to as the *"saddle point"* problem for the optimization problem, which means that the result becomes stuck at the local optimal point. The gradient information in (6) is reduced due to the low sampling rate, resulting in saddle points. Luckily, these saddle points are close to the true value. In the next set of simulations, the results of our proposed method are acceptable for N_s ranging from 0.1 to 0.9.

C. Overall Performance for Various N_s

In the previous section, we find that N_s may influence the result for both the MLE and NLS methods. To determine the robustness of our proposed method, we assess the performance under different nominal symbol rates. We evaluate 3×10^5 realizations for 9 different N_s ranging from 0.1 to 0.9 for $\beta = \{0.01, 0.1\}$. The OSNR is set to 10 dB.
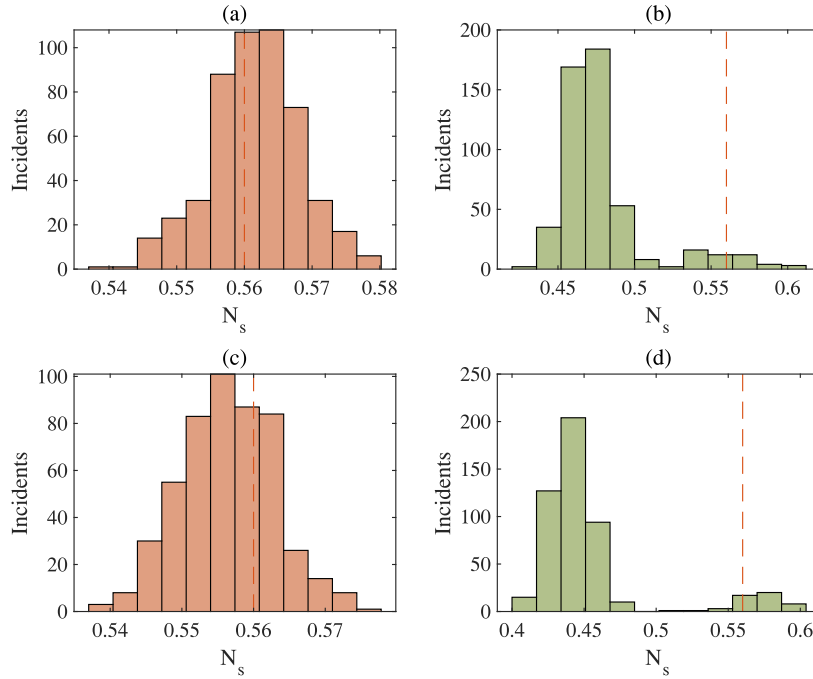
Fig. 13. Histogram of the proposed NLS method and maximum Likelihood estimator in [9]: (a) back-to-back, our proposed method; (b) back-to-back, MLE; (c) 3600 km, our proposed method; and (d) 3600 km, MLE.
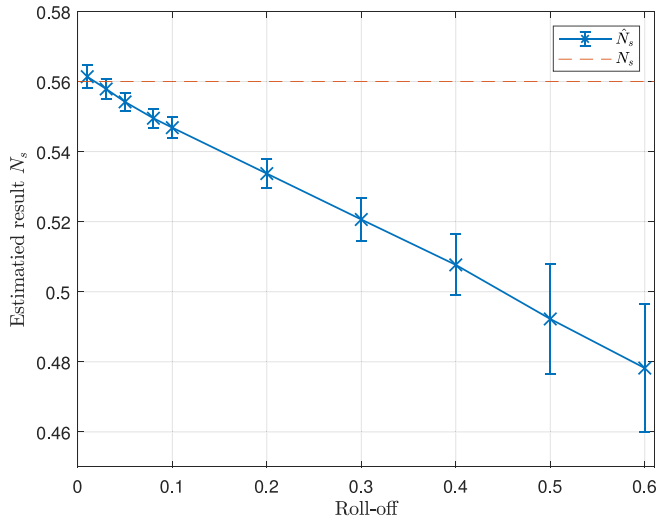

Fig. 14. Estimated nominal symbol rate $\hat{N}_s$ with error bars under different roll-off factors. Data points of crosses are averages of estimation while error bars represent standard deviations of the estimation results. The true value N_s is given as benchmark in red.

Fig. 15. Estimated nominal symbol rate $\hat{N}_s$ with error bars under different symbol rates. Data points of crosses are averages of estimation while error bars represent ranges of estimation results $\hat{N}_s$. The true value N_s is given as benchmark in red.

We have two major observations from Fig. 10. First, our proposed method has consistent performance for all N_s, while the MLE method fails to yield a reasonable result for $N_s > 0.5$. Although both methods use coarse and fine search steps, the MLE method works in a cascade manner, while the NLS method uses only coarse estimation in the initialization. Moreover, both stages of the MLE suffer from the aliasing problem. Our proposed method significantly outperforms the MLE for $N_s > 0.5$.

Second, the MLE method outperforms our proposed method for $\beta = 0.1$. The results also support the conclusion in the last part. When $N_s = 0.2$, the outlier performance and MSE performance are better for the MLE method.

D. Experimental Results

Further transmission experiments are carried out, as shown in Fig. 11. At the transmitter, external cavity laser (ECL,

model: TTX1994) with less than 100 kHz linewidth generates 194.1 THz carrier. The DP I/Q-modulator is driven by signals generated from a four-channel digital-to-analog converters (DAC) operating at a sample rate of 64 GSa/s and 8 b nominal resolution. The pulse shape is a square-root-raised cosine with $\beta = 0.01$. Then, the signal is amplified to 2 dBm before launching it into a fiber circulating loop. The link loop consists of a span of 80 km standard single-mode fibers with an average dispersion parameter of 16.75 ps/(km · nm). The power loss is fully compensated with an erbium-doped fiber amplifier. After the transmission, the signal is filtered by an optical bandpass filter of 0.4 nm before being sent into an integrated coherent receiver. The local oscillator is the same TTX1994. Finally, the signal is sampled with a real-time oscilloscope with 50 GSa/s sampling rate and 16 GHz bandwidth.

In the symbol rate estimation stage, a total of 3×10^6 samples are recorded to compare these two methods. For each evaluation, 3000 samples are used as the input sample for both our proposed method and the MLE method. Fig. 12 and Fig. 13 show the estimation performance versus various transmission lengths. The same algorithm setup is used as in the simulation part. The NLS method yields similar results to those of the simulation first investigated.

The proposed method tolerates fiber impairments up to 3600 km. The MLE method has a large bias compared to our proposed method. Although the sample length of 3000 is sufficient in the simulation to obtain a plausible result since the MLE cannot generate a cyclic correlation peak, the bandwidth of the oscilloscope limits the second-order cyclostationary component. As shown in Fig. 13(b) and Fig. 13(d), the cyclic correlation peak could not be generated by the MLE method.

In addition, the investigation to the performance under different roll-off factors is shown in Fig. 14. 28 GBaud Nyquist shaping PDM-16QAM signals are transmitted back to back with 50 GSa/s sampling in receiver. It's obvious that the proposed method estimates symbol rate quite precisely in low roll-off region as theory indicates, whereas $\hat{N}_s$ presents a linear fall and exceeds tolerance when roll-off factor climbs over 0.1. Low variance with accurate average of estimation under low roll-off factor proves reliability of NLS method.

Despite estimation results of various N_s given in Section 5.2, the universality of proposed scheme under different symbol rates in Nyquist shaping is verified. Comparison of N_s for 4 GBaud, 8 GBaud, 14 GBaud, 20 GBaud, 28 GBaud and 32 GBaud PDM-16QAM experiments with the same 50 GSa/s samlping rate and 0.05 roll-off Nyquist shaping is depicted above in Fig. 15. As depicted, estimation is accurate with averages of $\hat{N}_s$ all close to theoretical symbol rates. In the meanwhile, the performance is quite robust. Even maximum and minimum errors lead to no more than 1 GHz offset in case of 32 GHz. This 3% error obtained is accurate enough to distinguish between a set of baud-rates and the FEC level, where typical FEC overheads range between 6.69-25%[40], [41]. Compared to the method in [40] where up to 2% error is depicted in QPSK experiment with 2^{15} processed samples, our method can even reach a comparable error level in 16QAM system with only 3000 points. Therefore,

the precise NLS method is also practical for variable symbol rates.

VI. CONCLUSION

This paper proposed a nonlinear least squares method to estimate the symbol rate for the Nyquist WDM signal. For nominal symbol rates ranging from 0.1 to 0.9, the proposed method shows robust performance. For OSNRs as low as 12 dB, only 3000 samples are needed for robust symbol rate estimation with an MSE below 10^{-4}. The proposed NLS estimator was compared with the MLE method. The results show that the NLS method tolerates fiber impairments well. The method can be used in long-haul and low roll-off Nyquist WDM applications for its low computation complexity and high estimation precision.

APPENDIX A

For a strict band-limit signal with bandwidth B, the difference in the sample autocorrelation for timing offsets ϵ_1 and ϵ_2 can be expressed as:

$$
\begin{aligned}
d(k) &= \hat{r}_{xx,\epsilon_1}(k) - \hat{r}_{xx,\epsilon_2}(k) \\
&\propto \sum_{i=-\infty}^{\infty} g(iT_s/q + \epsilon_1)g(iT_s/q + kT_s + \epsilon_1)g(iT_s/q \\
&\quad + \epsilon_2)g(iT_s/q + kT_s + \epsilon_2) \\
&= \text{DTFT}\{g(t + \epsilon_1)g(t + \Delta + \epsilon_1) \\
&\quad - g(t + \epsilon_2)g(t + \Delta + \epsilon_2)\}|_{\omega=0} \\
&\doteq \text{DTFT}\{v(t)\}|_{\omega=0}.
\end{aligned}
\tag{10}
$$

where $\hat{r}_{xx,\epsilon}(k)$ denotes the sample autocorrelation with the timing offset ϵ, $t = iT_s/q$, and $\Delta = kTs$. We can see from (10) that $d(k)$ is a sampled average sum of $v(t)$ with the sampling interval T_s/q, which can be regarded as the discrete time Fourier transform (DTFT) at a frequency of 0.

Let $V(\omega)$ be the Fourier transform of $v(t)$:

$$
\begin{aligned}
|V(\omega)| &= |(e^{-j\omega\epsilon_1} - e^{-j\omega\epsilon_2})[G(\omega) * G(\omega)e^{-j\omega\Delta}]| \\
&= |1 - e^{-j(\epsilon_1-\epsilon_2)\omega}||G(\omega) * G(\omega)e^{-j\omega\Delta}|.
\end{aligned}
\tag{11}
$$

If $\omega = 0$ in (11), then $V(0) = 0$. $d(k)$ in (10) depends on the equivalent sampling rate and the bandwidth of $v(t)$. It is straightforward to show that when $N_s < 1$, the equivalent sampling ratio of the limit sample correlation $q \geq 2$. Using the well-known sampling relation:

$$
\begin{aligned}
d(k) = V_d(\omega)|_{\omega=0} &= \frac{q}{T_s} \sum_{n=-\infty}^{\infty} V\left(j\frac{q\omega}{T_s} - j\frac{2\pi qn}{T_s}\right)|_{\omega=0} \\
&\propto \sum_{n=-\infty}^{\infty} V\left(j\frac{2\pi qn}{T_s}\right).
\end{aligned}
\tag{12}
$$

Since $g(t)$ is a strict band-limit signal, $G(\omega)$ will have finite support on $[-(1 + \beta)/T, (1 + \beta)/T]$. The time-shift correlation part $|G(\omega) * G(\omega)e^{-j\omega\Delta}|$ is also finitely supported on $[-2(1 + \beta)/T, 2(1 + \beta)/T]$.

The worst case for aliasing is $\beta = 1$. Substituting $q \geq 2$ into (12), we have:

$$\frac{2\pi q n}{T_s} \geq \frac{2\pi q}{T_s} \geq \frac{4\pi}{T}. \tag{13}$$

and no aliasing will occur for all $n \geq 1$ in (12) at a frequency of 0, i.e., $d(k) = 0$.

REFERENCES

[1] X. Zhou, L. Nelson, and P. Magill, "Rate-adaptable optics for next generation long-haul transport networks," *IEEE Commun. Mag.*, vol. 51, no. 3, pp. 41–49, Mar. 2013.

[2] I. Tomkos, S. Azodolmolky, J. Sole-Pareta, D. Careglio, and E. Palkopoulou, "A tutorial on the flexible optical networking paradigm: State of the art, trends, and research challenges," *Proc. IEEE*, vol. 102, no. 9, pp. 1317–1337, Sep. 2014.

[3] G. H. Gho and J. M. Kahn, "Rate-adaptive modulation and coding for optical fiber transmission systems," *J. Lightw. Technol.*, vol. 30, no. 12, pp. 1818–1828, Jun. 2012.

[4] W. A. Gardner, A. Napolitano, and L. Paura, "Cyclostationarity: Half a century of research," *Signal Process.*, vol. 86, no. 4, pp. 639–697, 2006.

[5] F. N. Hauske, N. Stojanovic, C. Xie, and M. Chen, "Impact of optical channel distortions to digital timing recovery in digital coherent transmission systems," in *Proc. 12th Int. Conf. Transp. Opt. Netw.*, 2010, pp. 2–5.

[6] X. Zhou and L. Nelson, "Advanced DSP for 400 Gb/s and beyond optical networks," *J. Lightw. Technol.*, vol. 32, no. 16, pp. 2716–2725, Aug. 2014.

[7] M. Ionescu, M. Sato, and B. Thomsen, "Cyclostationarity-based joint monitoring of symbol-rate, frequency offset, CD and OSNR for nyquist WDM superchannels," *Opt. Exp.*, vol. 23, no. 20, 2015, Art. no. 25762. [Online]. Available: https://www.osapublishing.org/abstract.cfm?URI=oe-23-20-25762

[8] J. Ba, Z. Huang, Z. Zuo, and J. Wei, "Blind symbol rate estimation using nonlinearity on sample correlation for digital coherent systems," *Opt. Commun.*, vol. 451, pp. 246–254, Nov. 2019.

[9] C. Mosquera, S. Scalise, and R. López-Valcarce, "Non-data-aided symbol rate estimation of linearly modulated signals," *IEEE Trans. Signal Process.*, vol. 56, no. 2, pp. 664–674, Feb. 2008.

[10] Y. Zhou, A. Nirmalathas, T. B. Anderson, K. Clarke, and K. L. Lee, "Bitrate identification using asynchronous delayed sampling," *IEEE Photon. Technol. Lett.*, vol. 21, no. 13, pp. 893–895, Jul. 2009.

[11] S. Cui, S. Jin, W. Xia, C. Ke, and D. Liu, "Improved symbol rate identification method for on-off keying and advanced modulation format signals based on asynchronous delayed sampling," *Opt. Commun.*, vol. 354, pp. 218–224, 2015.

[12] J. Wei, Z. Dong, Z. Huang, and Y. Zhang, "Symbol rate identification for auxiliary amplitude modulation optical signal," *Opt. Commun.*, vol. 374, pp. 84–91, Sep. 2016.

[13] F. N. Khan, Y. Zhou, Q. Sui, and A. P. T. Lau, "Non-data-aided joint bit-rate and modulation format identification for next-generation heterogeneous optical networks," *Opt. Fiber Technol.*, vol. 20, no. 2, pp. 68–74, 2014.

[14] M. C. Tan, F. N. Khan, W. H. Al-Arashi, Y. Zhou, and A. P. Tao Lau, "Simultaneous optical performance monitoring and modulation format/bitrate identification using principal component analysis," *J. Opt. Commun. Netw.*, vol. 6, no. 5, pp. 441–448, May 2014.

[15] L. Guesmi, A. M. Ragheb, H. Fathallah, and M. Menif, "Experimental demonstration of simultaneous modulation format/symbol rate identification and optical performance monitoring for coherent optical systems," *J. Lightw. Technol.*, vol. 36, no. 11, pp. 2230–2239, Jun. 2018.

[16] R. D. Gitlin and J. F. Hayes, "Timing recovery and scramblers in data transmission," *Bell Syst. Tech. J.*, vol. 54, no. 3, pp. 569–593, 1975.

[17] J. E. Mazo, "Jitter comparison of tones generated by squaring and by fourth-power circuits," *Bell Syst. Tech. J.*, vol. 57, no. 5, pp. 1489–1498, 1978.

[18] S. Pupolin and C. Tomasi, "Spectral analysis of line regenerator time jitter," *IEEE Trans. Commun.*, vol. TCOMM-32, no. 5, pp. 561–566, May 1984.

[19] W. A. Gardner, "The role of spectral correlation in design and performance analysis of synchronizers," *IEEE Trans. Commun.*, vol. TCOMM-34, no. 11, pp. 1089–1095, Nov. 1986.

[20] C. Spooner and W. Gardner, "Robust feature detection for signal interception," *IEEE Trans. Commun.*, vol. 42, no. 5, pp. 2165–2173, May 1994.

[21] J.-C. Imbeaux, "Performances of the delay-line multiplier circuit for clock and carrier synchronization in digital satellite communications," *IEEE J. Sel. Areas Commun.*, vol. JSAC-1, no. 1, pp. 82–95, Jan. 1983.

[22] A. Dandawate and G. Giannakis, "Statistical tests for presence of cyclostationarity," *IEEE Trans. Signal Process.*, vol. 42, no. 9, pp. 2355–2369, Sep. 1994.

[23] L. Mazet and P. Loubaton, "Cyclic correlation based symbol rate estimation," in *Proc. Conf. Rec. 33rd Asilomar Conf. Signals, Syst., Comput.*, vol. 2, 1999, pp. 1008–1012.

[24] P. Ciblat, P. Loubaton, E. Serpedin, and G. Giannakis, "Asymptotic analysis of blind cyclic correlation-based symbol-rate estimators," *IEEE Trans. Inf. Theory*, vol. 48, no. 7, pp. 1922–1934, Jul. 2002.

[25] J. Y. Lee, Y. M. Chung, and S. U. Lee, "On a timing recovery technique for a variable symbol rate signal," in *Proc. IEEE Veh. Technol. Conf.*, vol. 3, 1997, pp. 1724–1728.

[26] Z. Yu, Y. Q. Shi, and W. Su, "Symbol-rate estimation based on filter bank," in *Proc. IEEE Int. Symp. Circuits Syst.*, 2005, pp. 1437–1440.

[27] H. Wymeersch and M. Moeneclaey, "Blind symbol rate detection for low-complexity multi-rate receivers," in *Proc. IEEE 61st Veh. Technol. Conf.*, vol. 2, 2005, pp. 1171–1175.

[28] J. Proakis and M. Salehi, *Digital Communications*, 5th ed. New York, NY, USA: McGraw-Hill, 2007. [Online]. Available: http://www.amazon.com/Digital-Communications-Edition-John-Proakis/dp/0072957166

[29] H. Li and Q. Cheng, "Almost sure convergence analysis of mixed time averages and kth-order cyclic statistics," *IEEE Trans. Inf. Theory*, vol. 43, no. 4, pp. 1265–1268, Jul. 1997.

[30] H. Meyr, M. Moeneclaey, and S. A. Fechtel, *Digital Communication Receivers: Synchronization, Channel Estimation, and Signal Processing*. New York, NY, USA: Wiley, Oct. 2001, doi: 10.1002/0471200573

[31] K. Kikuchi, "Fundamentals of coherent optical fiber communications," *J. Lightw. Technol.*, vol. 34, no. 1, pp. 157–179, Jan. 2016.

[32] P. Poggiolini, "The GN model of non-linear propagation in uncompensated coherent optical systems," *J. Lightw. Technol.*, vol. 30, no. 24, pp. 3857–3879, 2012.

[33] A. V. Oppenheim and R. W. Schafer, *Discrete Time Signal Processing*, 2nd ed. Englewood Cliffs, NJ, USA: Prentice-Hall, 1998.

[34] D. Zibar et al., "Experimental investigation and digital compensation of DGD for 112 gb/s PDM-QPSK clock recovery," *Opt. Exp.*, vol. 19, no. 26, pp. B429–B439, 2011.

[35] J. Lopez-Salcedo and G. Vazquez, "Fyequency domain iterative pulse shape estimation based on second-order statistics," in *Proc. IEEE 5th Workshop Signal Process. Adv. Wireless Commun.*, 2004, pp. 92–96. [Online]. Available: http://ieeexplore.ieee.org/document/1439210/

[36] J. J. Moré and D. C. Sorensen, "Computing a trust region step," *SIAM J. Sci. Stat. Comput.*, vol. 4, no. 3, pp. 553–572, Sep. 1983.

[37] S. M. Kay, *Fundamentals of Statistical Signal Processing: Estimation Theory*. Englewood Cliffs, NJ, USA: Prentice-Hall, 1968, vol. 1, pp. 289–299.

[38] M. Flohberger, W. Kogler, W. Gappmair, and O. Koudelka, "Symbol rate estimation with inverse Fourier transforms," in *Proc. Int. Workshop Satell. Space Commun.*, 2006, pp. 110–113.

[39] H. Xu, Y. Zhou, and Z. Huang, "Blind roll-off factor and symbol rate estimation using IFFT and least squares estimator," in *Proc. Int. Conf. Wireless Commun. Netw. Mobile Comput.*, 2007, pp. 1052–1055.

[40] M. Ionescu, M. Erkilinc, M. Paskov, S. Savory, and B. Thomsen, "Novel baud-rate estimation technique for M-PSK and QAM signals based on the standard deviation of the spectrum," in *Proc. 39th Eur. Conf. Exhib. Opt. Commun.*, 2013, pp. 1–3.

[41] T. Mizuochi, "Next generation FEC for optical communication," in *Proc. Opt. Fiber Commun. Conf./Nat. Fiber Opt. Eng. Conf.*, 2008, paper OTuE5.